Kinetics and mechanism of hydroxyl radical reaction with methyl hydroperoxide

ARTICLE *in* THE JOURNAL OF PHYSICAL CHEMISTRY · MARCH 1989

Impact Factor: 2.78 · DOI: 10.1021/j100342a050

2 AUTHORS:

Ghanshyam Vaghjiani
United States Air Force
60 PUBLICATIONS **1,471** CITATIONS
SEE PROFILE

A.R. Ravishankara
Colorado State University
508 PUBLICATIONS **18,473** CITATIONS
SEE PROFILE

Kinetics and Mechanism of OH Reaction with CH_3OOH

Ghanshyam L. Vaghjiani and A. R. Ravishankara*

Aeronomy Laboratory, National Oceanic and Atmospheric Administration, Boulder, Colorado 80303, and the Cooperative Institute for Research in Environmental Sciences, University of Colorado, Boulder, Colorado 80309 *(Received: July 12, 1988)*

The reaction of hydroxyl radical with methyl hydroperoxide, CH_3OOH, was investigated in the temperature range 203–423 K by pulsed photolytic generation of OH and detection by laser-induced fluorescence. The rate coefficient for the overall reaction, $OH + CH_3OOH \rightarrow$ products (k_1) was measured by using ^{18}OH and OD in place of OH. The rate coefficient for the CH_3O_2 production channel $OH + CH_3OOH \rightarrow CH_3O_2 + H_2O$ (k_{1a}) was obtained by using OH. The channel that yields CH_2OOH, $OH + CH_3OOH \rightarrow CH_2OOH + H_2O$ (k_{1b}), is not observed when monitoring OH since CH_2OOH rapidly falls apart to give back OH (and CH_2O) but is observed when studying the ^{18}OH or OD reaction with CH_3OOH. By monitoring OH production in $OD + CH_3OOH$ reaction at 249 K, the two-channel mechanism was confirmed, and the values for k_1 and k_{1a} were also determined. Both reaction 1 and channel 1a show negative activation energies, with $k_1 = (2.93 \pm 0.30) \times 10^{-12} \exp((190 \pm 14)/T)$ cm^3 molecule^{-1} s^{-1} (average of ^{18}OH and OD studies) and $k_{1a} = (1.78 \pm 0.25) \times 10^{-12} \exp((220 \pm 21)/T)$ cm^3 molecule^{-1} s^{-1}, where the indicated error is 1σ, including estimated systematic errors and $\sigma_A = A\sigma_{\ln A}$. The rate coefficient for the reaction of OD with CH_3OOD is at least a factor of 2 smaller than that for reaction 1a. The thermal decomposition lifetime for CH_2OOH to give $OH + CH_2O$ is deduced to be shorter than 20 μs at 205 K. The mechanism of reaction 1 and the implications of our kinetic and mechanistic results to Earth's atmospheric chemistry are discussed. The measured value of k_1 and the branching ratio, k_{1a}/k_{1b}, at 298 K are compared with previous indirect measurements of Niki et al. [*J. Phys. Chem.* **1983**, *87*, 2190].

Introduction

Methyl hydroperoxide, CH_3OOH, is an important intermediate in the atmospheric oxidation of methane[1,2] and nonmethane hydrocarbons.[3] It is believed to be formed in the low-temperature combustion of hydrocarbons.[4] The effect of CH_3OOH formation on atmospheric and combustion systems depends on the rate of its formation, the rate of its removal, the products of removal reactions, and its steady-state concentration. Reaction of CH_3O_2 with HO_2 generates CH_3OOH:

$$CH_3O_2 + HO_2 \rightarrow CH_3OOH + O_2$$

The rate coefficient for this reaction has been measured by various investigators,[5-9] and it is uncertain by a factor of 2 at 298 K. The overall uncertainty in this rate coefficient under atmospheric pressure and temperature conditions is likely to be a factor of 3. This rate coefficient has a negative temperature dependence[6,8] and is independent of pressure.[5,7]

The processes that remove CH_3OOH in the atmosphere are its reaction with OH:

$$CH_3OOH + OH \rightarrow \text{products} \quad (1)$$

its photolysis:

$$CH_3OOH + h\nu \rightarrow \text{products} \quad (2)$$

and scavenging by water droplets. In combustion systems, reactions of $O(^3P)$ and $H(^2S)$

$$CH_3OOH + O(^3P) \rightarrow \text{products} \quad (3)$$

$$CH_3OOH + H(^2S) \rightarrow \text{products} \quad (4)$$

along with the thermal decomposition and reaction 1 are important. Of all the removal processes due to free-radical reactions, reaction 1 is expected to be the most important, but its rate coefficient is also the least certain.

The rate coefficient for reaction 1, k_1, determines the atmospheric concentration of CH_3OOH. It is necessary to know the gas-phase concentration of CH_3OOH in the atmosphere since the amount of CH_3OOH that can be transported in the liquid phase (i.e., water droplets in clouds) depends on it. In solution, CH_3OOH is a potential oxidizer of SO_2 to sulfuric acid.[10] Under certain conditions CH_3OOH in solution can oxidize as much SO_2 as the gas-phase mechanism, via the $OH + SO_2$ reaction, in the troposphere. It is also necessary to know the value of k_1 to understand the effect of CH_3OOH on the concentration of odd hydrogen radicals, HO_x, in the troposphere[2] and the Antarctic stratosphere during the austral spring[11] due to methane oxidation.

If reaction 1 proceeds via an H-atom abstraction, it has two possible channels:

$$OH + CH_3OOH \xrightarrow{k_{1a}} CH_3O_2 + H_2O \quad (1a)$$

$$OH + CH_3OOH \xrightarrow{k_{1b}} CH_2OOH + H_2O \quad (1b)$$

CH_2OOH is expected to be very unstable and to fall apart to give CH_2O and OH:

$$CH_2OOH \xrightarrow[M]{k_c} CH_2O + OH \quad (5)$$

The path by which CH_3OOH reacts with OH, i.e., (1a) or (1b), has a large influence on the effect of methane oxidation on atmospheric HO_x concentration where CH_4 oxidation is the dominant HO_x source. Reaction 1a leads to a lower HO_x production than does reaction 1b in the CH_4 oxidation scheme.[2]

CH_3OOH is the simplest organic peroxide. It is very similar to H_2O_2, whose reaction with OH is well studied.[12] Therefore, it is interesting to investigate how the methyl group affects the

* Address correspondence to this author at NOAA/ERL, R/E/AL2, 325 Broadway, Boulder, CO 80303.

(1) Levy II, H. *Planet. Space Sci.* **1972**, *20*, 919. Levy II, H. *Planet. Space Sci.* **1973**, *21*, 575.
(2) Logan, J. A.; Prather, M. J.; Wofsy, S. C.; McElroy, M. B. *J. Geophys. Res.* **1981**, *86*, 7210.
(3) Trainer, M.; Hsie, E. Y.; McKeen, S. A.; Tallamraju, R.; Parrish, D. D.; Fehsenfeld, F. C.; Liu, S. C. *J. Geophys. Res.* **1987**, *92*, 11879.
(4) Walker, R. W. In *Specialist Periodical Reports. Reaction Kinetics*; Ashmore, P. G., Ed.; The Chemical Society: London, 1975; Vol. 1, p 161.
(5) McAdam, K.; Veyret, B.; Lesclaux, R. *Chem. Phys. Lett.* **1987**, *133*, 39.
(6) Cox, R. A.; Tyndall, G. S. *J. Chem. Soc., Faraday Trans. 2* **1980**, *76*, 153.
(7) Kurylo, M. J.; Dagaut, P.; Wallington, T. J.; Neuman, D. M. *Chem. Phys. Lett.* **1987**, *139*, 513.
(8) Dagaut, P.; Wallington, T. J.; Kurylo, M. J. *J. Phys. Chem.* **1988**, *92*, 3833.
(9) Moortgat, G. K.; Burrows, J. P.; Schneider, W.; Tyndall, G. S.; Cox, R. A. Proceedings of the 4th European Symposium on Physico-chemical Behavior of Atmospheric Pollutants, 1986; pp 271–281.
(10) Calvert, J. G.; Lazrus, A.; Kok, G. L.; Heikes, B. G.; Walega, J. G.; Lind, J.; Cantrell, C. A. *Nature* **1985**, *317*, 27.
(11) Crutzen, P. J.; Arnold, F. *Nature* **1986**, *324*, 651.
(12) DeMore, W. B.; Watson, R. T.; Golden, D. M.; Hampson, R. F.; Kurylo, M. J.; Howard, C. J.; Molina, M. J.; Ravishankara, A. R. *Chemical Kinetics and Photochemical Data for use in Stratospheric Modeling*; Evaluation No. 5, JPL Publication 82-57, 1982.

0022-3654/89/2093-1948$01.50/0

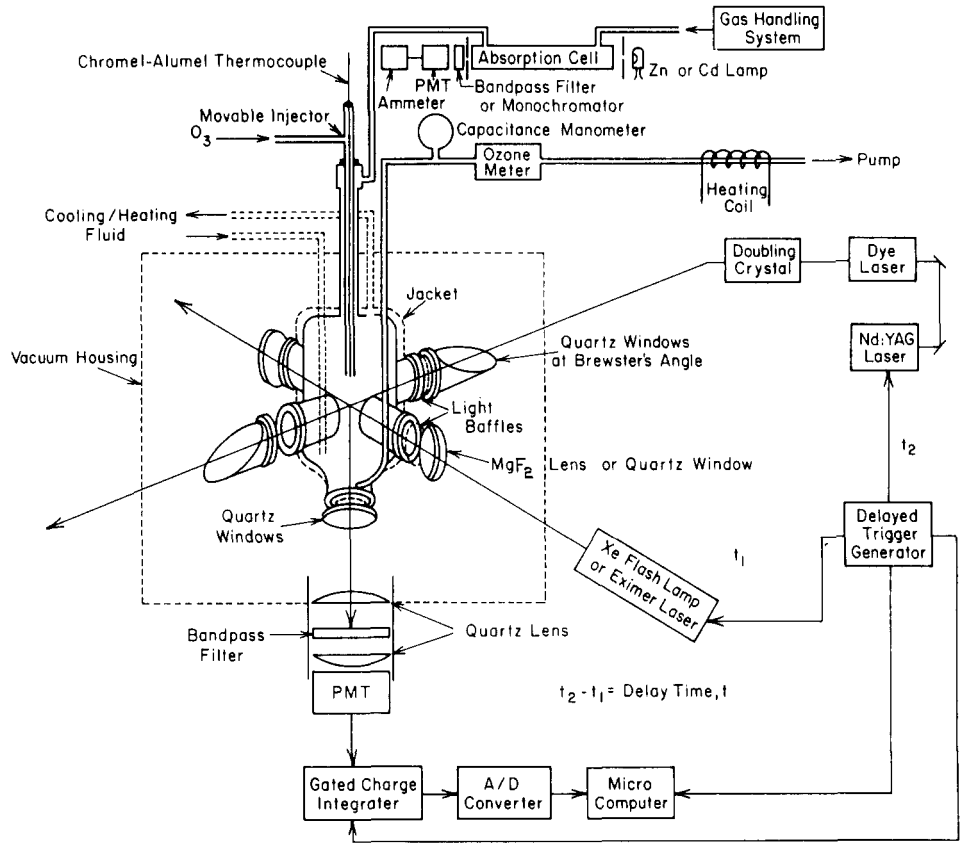

Figure 1. Schematic diagram of the apparatus used to study kinetics and mechanism of reaction 1.

reactivity with OH. Such an investigation would help predict rate coefficients for more complex organic peroxides once the mechanisms and rates of the reaction are understood.

Due to the above reasons, it is important to know the values of k_1, k_{1a}, and k_{1b} accurately. By analogy with OH + H_2O_2 and OH + CH_3OH reactions, k_1 at 298 K was estimated[13] to be approximately 1×10^{-12} cm^3 molecule^{-1} s^{-1}. However, in the only investigation of reaction 1, Niki et al.[14] obtained a value of $k_1 = 1 \times 10^{-11}$ cm^3 molecule^{-1} s^{-1} at 298 K, using a competitive method in a chamber experiment. They also deduced k_{1a}/k_{1b} to be ~1.3 at 298 K. These measurements require confirmation. The temperature dependencies of k_1, k_{1a}, and k_{1b} are unknown. Therefore, we have carried out direct measurements of k_1, k_{1a}, and k_{1b} between 203 and 423 K.

Experimental Section

The apparatus used in the present study is similar to the one used in previous OH reaction studies in our laboratory, and it is schematically shown in Figure 1. The reaction vessel was a Pyrex-jacketed cell with an internal volume of ~150 cm^3 and was housed in a vacuum chamber. The cell was maintained at a desired constant temperature (±1 K) by circulating thermostated fluid through its outer jacket. The temperature of the gases in the cell was measured by a chromel–alumel thermocouple located inside the reactor just above the volume where hydroxyl radicals were generated. A gas mixture containing CH_3OOH, photolytic precursors, and the bath gas flowed through the cell with a linear velocity in the range 2–15 cm s^{-1}. Composition of the mixture was calculated from mass flow rates measured by using calibrated mass flow meters, the pressure in the cell, and UV absorptions of CH_3OOH and O_3. The methyl hydroperoxide was introduced into the cell by saturating a small flow of helium buffer gas through a glass bubbler containing anhydrous methyl hydroperoxide maintained at 273 K. The cell pressure was measured by using a capacitance monometer. Methyl hydroperoxide concentration in the mixture flowing through the cell was directly measured by 213.9-nm absorption in a 100-cm-long cell maintained at room temperature. The 213.9-nm line from a zinc lamp was isolated by using a band-pass filter (peak transmission at 211.4 nm and a full width at half-maximum, fwhm, of 17.7 nm) and detected by a photomultiplier tube. The absorption cross section used was $\sigma_{213.9} = 2.25 \times 10^{-19}$ cm^2 molecule^{-1} at 298 K. In a few cases methyl hydroperoxide concentration was determined by monitoring the attenuation of the 228.8-nm cadmium line isolated by using a 0.25-m monochromator. The value of the absorption cross section used was $\sigma_{228.8} = 1.00 \times 10^{-19}$ cm^2 molecule^{-1}. These are the absorption cross sections determined in our laboratory[15] and are different from the ones reported by Molina and Arguello.[16] Justification for using these values is given later. The methyl hydroperoxide concentration in the gas mixture was determined either before the mixture entered the reaction cell or, in some cases, just after the mixture exited the reaction cell. The methyl hydroperoxide concentration in the cell was corrected for differences in temperature between the reactor and the absorption cell. To reduce the extent of decomposition of methyl hydroperoxide, either Pyrex or Teflon tubing was used throughout the gas-handling manifold, except for a few stainless steel fittings.

OH free radicals were generated by pulsed photolysis of a suitable precursor. Several hydroxyl radical precursors were used in the present study. These are summarized in Table I.

The concentration of the hydroxyl radical was monitored by pulsed laser-induced fluorescence (LIF). The second harmonic of a Nd:YAG laser (532 nm) was used to pump a tunable dye laser. The output of the dye laser was frequency doubled to obtain wavelengths around 280–290 nm. The dye laser was tuned to pump the $Q_1(1)$ line, and in some cases $Q_1(2)$, $Q_1(3)$, and $R_1(3)$ lines, in the (1,0) band of the ($A^2\Sigma^+, v'=1$) ← ($X^2\Pi, v''=0$) transition of the hydroxyl radical. All three isotopic hydroxyl

(13) DeMore, W. B.; Margitan, J. J.; Molina, M. J.; Watson, R. J.; Golden, D. M.; Hampson, R. F.; Kurylo, M. J.; Howard, C. J.; Ravishankara, A. R. *Chemical Kinetics and Photochemical Data for Use in Stratospheric Modeling*; Evaluation No. 7, JPL Publication 85-37, 1985.

(14) Niki, H.; Maker, P. D.; Savage, C. M.; Breitenbach, L. P. *J. Phys. Chem.* **1983**, *87*, 2190.

(15) Vaghjiani, G. L.; Ravishankara, A. R. *J. Geophys. Res.*, submitted for publication.

(16) Molina, M. J.; Arguello, G. *Geophys. Res. Lett.* **1979**, *6*, 953.

TABLE I: Photolytic Sources of Hydroxyl Radicals Used in the Present Study

hydroxyl radical	reaction scheme	radiation source[a]
OH	1. $H_2O + h\nu \rightarrow OH + H$	1 (a)
	2. $CH_3OOH + h\nu \rightarrow CH_3O + OH$	1 (c), 2
	3. $O(^1D) + H_2O \rightarrow 2OH$	3
OD	1. $D_2O + h\nu \rightarrow OD + D$	1 (b)
	2. $O(^1D) + D_2O \rightarrow 2OD$	3
	3. $O(^1D) + D_2 \rightarrow OD + D$ and $(D + O_3 \rightarrow OD + O_2)$[b]	3
^{18}OH	1. $H_2{}^{18}O + h\nu \rightarrow {}^{18}OH + H$	1 (a)
	2. $O(^1D) + H_2{}^{18}O \rightarrow {}^{18}OH + OH$	3

[a] 1. A xenon flash lamp, 0.1–1.5 J and 10-μs duration. The precursor was photolyzed in the following wavelength ranges: (a) 165 nm (quartz cut off) to 185 nm (H_2O absorption cut off); (b) 165–181 nm (D_2O absorption cut off); (c) for wavelength $\lambda > 165$ nm when the region between Xe flash lamp and the cell was flushed with N_2 and for $\lambda > \sim 190$ nm when the region was flushed with air. 2. A KrF excimer laser, 248 nm and 16-ns pulse duration, with 0.02–5 mJ cm^{-2} fluence. 3. $O(^1D)$ was made by laser photolysis of O_3 at 248 nm; $O_3 \xrightarrow{h\nu} O(^1D) + O_2(^1\Delta)$ (90%); $O_3 \xrightarrow{h\nu} O(^3P) + O_2(X^3\Sigma)$ (10%). [b] This reaction also took place when O_3 concentration was high; the vibrationally excited OD produced by this reaction is quenched by the large concentration of H_2O added to this system (see text).

radicals, OH, ^{18}OH, and OD, could be detected by using a single dye, rhodamine 590, in the laser. OH and ^{18}OH were probed at ~281.1 nm, and OD was probed at ~287.6 nm. The probe beam was passed through the reaction cell to intersect the photolysis beam in the reaction zone. The probe beam had a pulse width of ~8 ns (fwhm) and a line width (fwhm) of ~0.008 nm. The resultant fluorescence of the hydroxyl radical corresponding to $(A^2\Sigma^+,v'=1) \rightarrow (X^2\Pi,v''=1)$ and $(A^2\Sigma^+,v'=0) \rightarrow (X^2\Pi,v''=0)$ transitions was collected along the third orthogonal axis by using a lens system, passed though a band-pass filter (centered at 308.7 nm, with a fwhm of 5.9 nm) and imaged onto a photomultiplier tube. The band heads for the above fluorescence transitions for OH (and ^{18}OH) are at 312.2 and 306.4 nm, respectively, and for OD at 310.9 and 306.8 nm, respectively. The output pulse from the photomultiplier tube was fed to a gated charge integrator. The integrated signal (integration time ~200 ns) was fed to a microcomputer via an A/D (analog to digital converter) port for signal averaging. One hundred pulses were signal averaged to improve the signal-to-noise ratio. The magnitude of the averaged signal (which was directly proportional to the hydroxyl radical concentration) was determined for several different delay times, t, between the photolysis pulse and the probe pulse. Both the photolysis source and the probe laser were run at 10 Hz. The energies of the photolysis source and the probe laser were constant over the entire experiment, and it was not necessary to normalize the measured signal to either of the two energies.

The initial concentration of hydroxyl radical, 1×10^{10}–1×10^{12} molecules cm^{-3}, was at least 3 orders of magnitude smaller than that of methyl hydroperoxide, 2×10^{14}–2×10^{15} molecules cm^{-3}. In experiments where CH_3OOH was photolyzed by a KrF laser, the initial hydroxyl radical concentration was computed from the known absorption cross section at 248 nm, the measured laser fluence, and the measured concentration of CH_3OOH in the cell. The quantum yield for OH production at this wavelength has been determined to be near unity.[17] The concentration of hydroxyl radicals produced in the reaction $O(^1D) + H_2O \rightarrow 2OH$ during the laser photolysis of O_3/H_2O mixtures was obtained by calculating $[O(^1D)]$ and assuming that each $O(^1D)$ generates two OH radicals. When flash photolysis was used, actinometry experiments were carried out to determine the concentration of hydroxyl radicals produced during the broad-band xenon flash lamp photolysis of the precursor, H_2O or CH_3OOH. Ozone, 2×10^{13} molecules cm^{-3}, was photolyzed in the presence of water, 5×10^{15} molecules cm^{-3}, in excess He by using a known laser fluence at 248 nm. The initial OH signal was determined by extrapolating the decay of the signal to time zero, and the initial concentration calculated. The laser was replaced by the xenon flash lamp (1.5 J), and the same amount of water flash photolyzed in the range 165–185 nm. The cell geometry, probe beam energy, and cell pressure were unchanged. Comparison of the initial OH signal in this latter experiment to that determined in the former gave the initial amount of OH made. Flash photolysis of 5×10^{15} molecules cm^{-3} of H_2O produced $\sim 5 \times 10^{10}$ molecules cm^{-3} of OH. Similar actinometry experiments for flash photolysis ($\lambda > 165$ nm) of CH_3OOH were carried out by using 248-nm photolysis of CH_3OOH itself. It was determined that $\sim 6 \times 10^{10}$ molecules cm^{-3} of OH were produced during the flash photolysis of 2×10^{15} molecules cm^{-3} of CH_3OOH.

The temporal profiles of hydroxyl radical concentration in kinetic experiments were determined by measuring the LIF signal at various delay times between the photolysis pulse and the probe laser. The background signal, mostly due to OH generated by the probe laser and scattered laser beam light, was obtained by blocking the photolysis light. The background signal was subtracted from the hydroxyl radical signal produced by the photolysis beam. The former typically is a factor of 10–100 smaller compared to the latter signal due to OH produced in the initial photolysis. Normally 5–10 delay times were employed to define the decay rate of hydroxyl radicals. In some special cases where we were attempting to monitor nonexponential or double-exponential profiles, more delay times were employed to clearly define the profiles.

In one set of experiments, the rate coefficient for the quenching of $OH(A^2\Sigma^+)$ from the $v' = 0$ level to the ground $(X^2\Pi)$ state by CH_3OOH was measured by using SF_6 to rapidly quench $OH(A^2\Sigma^+)$ from the $v' = 1$ to $v' = 0$ level. The measurement was carried out in excess He, and the quenching rate coefficient obtained is for rotationally thermalized $OH(A^2\Sigma^+)$ radicals at 298 K. Details of this type of experiment can be found elsewhere.[28] The value for the quenching rate coefficient was $(1.10 \pm 0.08) \times 10^{-9}$ cm^3 molecule^{-1} s^{-1} (the error is 1σ, precision plus systematic).

Methyl hydroperoxide is not commercially available; therefore, it was synthesized by methylation of hydrogen peroxide.[18] A mixture of dimethyl sulfate (100 g, 0.79 mol), 30% hydrogen peroxide (150 mL), and water (250 mL), under continuous stirring, was treated dropwise with 40% potassium hydroxide solution (84 g, 1.5 mol, in 126 mL of water) at 273 K over a period of 40 min. Dimethyl peroxide, a byproduct of the reaction, escapes as a gas. After the addition of KOH solution, the mixture was acidified with 50% sulfuric acid at 273 K in a fume hood. The resultant solution was continuously extracted with diethyl ether over a period of several hours. The ether solution was dried over anhydrous sodium sulfate overnight and concentrated by boiling off the excess ether while maintaining the solution at 308 K with a water bath. The concentrated mixture was further dried over anhydrous copper sulfate. The raw product (~18 g) was fractionally distilled in a nitrogen atmosphere under reduced pressure at 323–333 K. The main fraction, with a vapor pressure of 65 Torr at 307–308 K, was collected to obtain 5 g of colorless liquid. Methyl hydroperoxide itself is stable at ambient conditions and is conveniently stored for long periods at 195 K in a Pyrex container equipped with a Teflon stopcock.

Caution: A pale yellow oily residue remained in the distillation flask. During one preparation, the residue violently exploded when dismantling the distillation apparatus, which had been exposed to air for 10–15 min. The apparatus was completely destroyed in the explosion. Reaction of the residue with O_2 and possible grinding of glassware are suspected to have caused the explosion. Quenching of the residue in water helps prevent such accidents.

The purity of the methyl hydroperoxide was checked by infrared and proton, ^{1}H, NMR analyses. The CH_3OOH vapor (10.0 Torr) was introduced into a 10-cm-long Pyrex cell fitted with KBr

(17) Vaghjiani, G. L.; Ravishankara, A. R. *J. Phys. Chem.*, submitted for publication.

(18) Rieche, A. *Alkylperoxyde Und Oxonide*; Theodor Steinkopff: Dresden, 1931; pp 12–13.

windows from a reservoir of degassed anhydrous liquid methyl hydroperoxide. The spectrum was recorded in the region 800–3800 cm^{-1} by using a Fourier transform spectrometer operating at 0.16-cm^{-1} resolution. A sharp singlet feature at 2963.8 cm^{-1} in the broad C–H stretch region at ~3000 cm^{-1} and a sharp triplet feature at 1346.5, 1332.4, and 1320.7 cm^{-1} in the broad C–H bend region at ~1350 cm^{-1} were identified. The measured absorption cross section at 2963.8 cm^{-1} with a resolution of 0.16 cm^{-1}, the same as that used by Niki et al.,[14] was 3.4×10^{-19} cm^2 $molecule^{-1}$, in agreement with the value reported by Niki et al. Liquid-phase ^1H NMR (in $CDCl_3$) of the prepared sample showed two features at chemical shifts, δ, of 8.86 ppm (broad, singlet, 1 H) assigned to the OH group and at 3.87 ppm (sharp, singlet, 3 H) assigned to the CH_3 group. The vapor pressure at 308 K was 65 Torr, in agreement with the literature value. The heat of vaporization for methyl hydroperoxide was determined to be 9.5 ± 0.6 kcal mol^{-1}. The indicated error is 1σ (precision only). The overall error in this value is estimated to be ~30% arising from systematic errors and the fact that the pressure measured for the vapor above the liquid peroxide may not truly correspond to that of a thermally equilibrated system. The purity of the sample when synthesized was greater than 96%. The major impurity is the extractant ether; ^1H NMR showed a trace of this compound, ~2–4%. Upon prolonged bubbling of helium or nitrogen through this liquid, it is expected to preferentially remove ether, and no lines due to ether were seen in the IR spectra. Before use, a diluent gas was bubbled through the sample for a few days. There was no noticeable change in the measured value of the rate coefficient over a period of several months.

Ozone was made by passing O_2 through a commercial ozonizer and stored over silica gel at 195 K. It was degassed at 77 K before use. H_2O was distilled in the laboratory. D_2O (99.8% D atom) from Merck Sharp and Dohme, Canada, $H_2{}^{18}O$ (>95% ^{18}O atom) from Monsanto Research, D_2 (>99.99%) from Alphagaz, O_2 (99.999%) and SF_6 (99.9%) from Scientific Gas Products, He (99.9996%) from U.S. Bureau of Mines, and N_2 (>99.998%) from Union Carbide were all used as supplied.

Results and Discussion

We have studied the reactions of CH_3OOH with ^{16}OH, ^{18}OH, and ^{16}OD. For convenience, ^{16}OH and ^{16}OD will be referred to as OH and OD, respectively, in the remainder of the paper. To appreciate the reasons for carrying out such isotopic substitutions and to understand our kinetic and mechanistic results, it is necessary to point out the assumed mechanism for reaction 1. As stated earlier, hydroxyl radicals can abstract hydrogen atoms from either the oxygen or the CH_3 group:

$$OH + CH_3OOH \xrightarrow{k_{1a}} CH_3O_2 + H_2O \qquad (1a)$$

$$OH + CH_3OOH \xrightarrow{k_{1b}} CH_2OOH + H_2O \qquad (1b)$$

CH_2OOH will quickly fall apart to give CH_2O and OH (this point will be discussed in detail later):

$$CH_2OOH \xrightarrow[M]{k_c} CH_2O + OH \qquad (5)$$

Methyl hydroperoxide contains essentially only ^{16}O isotope since H_2O_2 containing natural abundances of oxygen isotopes (99.76% ^{16}O, 0.04% ^{17}O, and 0.20% ^{18}O) was used in the preparation of CH_3OOH. Therefore, when the decay of [OH] is monitored in excess CH_3OOH, channel 1b is "dark" and we measure only k_{1a}. However, when ^{18}OH or OD are used, channel 1b followed by reaction 5 produces OH and hence the measured decay rates of [^{18}OH] and [OD] yield $k_{1a} + k_{1b}$. Any changes in the rate coefficients due to isotopic substitution (i.e., primary and secondary kinetic isotope effects) are very small and will be discussed later.

The possibility that OD and ^{18}OH undergo isotope exchange with CH_3OOH, i.e.

$$OD + CH_3OOH \rightleftarrows (CH_3OOH{\cdot}OD) \rightarrow CH_3OOD + OH$$

or

$$^{18}OH + CH_3OOH \rightleftarrows (CH_3OOH{\cdot}{}^{18}OH) \rightarrow CH_3O{}^{18}OH + OH$$

and that the measured [OD] and [^{18}OH] profiles do not yield $k_{1a} + k_{1b}$ exists; but as discussed later it is extremely unlikely. Another possible reaction is $CH_3OOH + OH \rightarrow CH_3O + H_2O_2$ (ΔH_r (298 K = −7.2 kcal mol^{-1}). This reaction path is indistinguishable from reaction 1a when monitoring [OH] temporal profiles. The measured rate coefficient will be a sum for these two reactions.

All kinetic experiments were carried out under pseudo-first-order conditions in the concentration of hydroxyl radicals. The CH_3OOH concentration exceeded the initial hydroxyl radical concentration by about a factor of 1×10^3. Therefore, the temporal profiles of the reactant hydroxyl radical concentration followed a simple first-order rate law, $[X]_t = [X]_0 \exp(-k't)$, where X = OH, OD, or ^{18}OH and $k' = k[CH_3OOH]$ + constant. k' is the pseudo-first-order rate coefficient for loss of X, the constant is the first-order rate coefficient for loss of X in the absence of CH_3OOH, and k is the second-order rate coefficient. k_1, k_{1a}, and, by difference, k_{1b} were measured in the temperature range 203–423 K. These measurements will be described first, followed by a discussion of the mechanistic studies.

Measurement of k_{1a}. OH + CH_3OOH. k_{1a} was measured by following the temporal profile of [OH]. OH was generated either by 248-nm KrF laser photolysis of CH_3OOH in the presence of H_2O, or by 165–185-nm photolysis of H_2O by a xenon flash lamp, or via the reaction of $O(^1D)$ with H_2O. The temporal profile of [OH] followed a single-exponential decay given by

$$[OH]_t = [OH]_0 e^{-k'_{1a}t} \qquad (I)$$

with

$$k'_{1a} = k_{1a}[CH_3OOH] + k_d{}^{OH}$$

k'_{1a} is the pseudo-first-order decay rate coefficient, and $k_d{}^{OH}$ is the first-order rate coefficient for the decay of [OH] in the absence of CH_3OOH. $[OH]_t$ and $[OH]_0$ are the concentrations of OH at time t and zero, respectively. As noted earlier, there is no contribution to measured [OH] decay by reaction 1b.

Figure 2c shows the temporal profiles of [OH] obtained at various CH_3OOH concentrations at 298 K. The decays were found to be exponential over at least 3 lifetimes. The straight lines represent a weighted linear least-squares fit to the data. The second-order rate coefficient, k_{1a}, for the reaction of OH with CH_3OOH was obtained from the slopes of plots of k'_{1a} versus [CH_3OOH]. One such plot derived at 298 K is shown in Figure 3. The straight line is a weighted linear least-squares fit to the data points. Measurements of k_{1a} were made at 203, 223, 244, 298, and 348 K. The results are summarized in Table II.

During the course of k_{1a} measurements, three separate sources of OH (shown in Table I) were used. Photolysis of H_2O in 165–185-nm region produces only $OH(X^2\Pi)$.[19] Any OH that is produced vibrationally excited is very rapidly quenched to $OH(X^2\Pi, v''=0)$ by H_2O.[20] The presence of a large concentration of diluent gas ensures thermalization of rotational levels. OH generated by $O(^1D) + H_2O$ reaction can also be vibrationally excited.[21] Here again, the presence of H_2O helps rapid thermalization of vibrational populations. In both these cases, presence of more than 1 Torr of H_2O ensured complete thermalization within ~10 μs, which is instantaneous compared to the time scale for the decay of [OH] due to reaction. In experiments where only CH_3OOH was photolyzed at 248 nm in He, we saw no evidence for significant production of vibrationally excited OH. The [OH] temporal profiles were strictly exponential, and the measured value of k_{1a} was the same as that obtained upon addition of 1 Torr of H_2O to the reaction mixture (H_2O is not photolyzed by 248-nm radiation and hence acts only as a quencher). This indicates either that vibrationally excited OH is not formed or that, if formed,

(19) Welge, K. H.; Stuhl, F. *J. Chem. Phys.* **1967**, *46*, 2440.
(20) Smith, I. W. M.; Williams, M. D. *J. Chem. Soc., Faraday Trans. 2* **1985**, *81*, 1849.
(21) Butler, J. E.; Tally, L. D.; Smith, G. K.; Lin, M. C. *J. Chem. Phys.* **1981**, *74*, 4501.

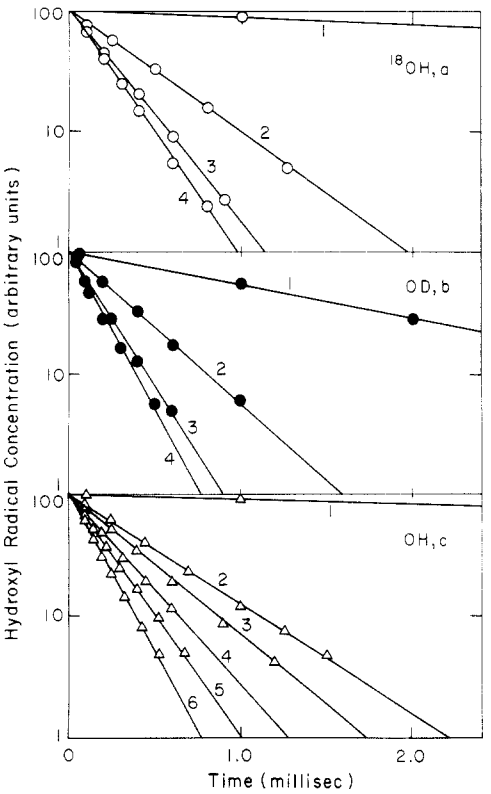

Figure 2. Typical plots of the hydroxyl radical concentrations (logarithmic scale) as a function of time at a few different CH_3OOH concentrations. Each line was obtained by measuring hydroxyl radical concentrations at up to 10 different reaction times; only a few points that cover the whole range of reaction time studied are shown for clarity. The slope of each plot was obtained by weighted linear least-squares procedure and yields the value of the pseudo-first-order rate coefficient, k'. The data shown were obtained at 298 K. In the absence of CH_3OOH, many data points at longer reaction times were taken; these cannot be shown in the figure. (a) ^{18}OH was produced by 165–185-nm photolysis of $H_2{}^{18}O$. The CH_3OOH concentrations are as follows: 1, 0; 2, 3.60×10^{14}; 3, 7.32×10^{14}; 4, 8.88×10^{14} molecules cm^{-3}. (b) OD was produced by the reaction $O(^1D) + D_2 \rightarrow OD(v''\leq 6) + D$ in $\sim 2 \times 10^{16}$ molecules cm^{-3} of H_2O. The rapid formation of $OD(v''=0)$ at short reaction times, <10 μs, due to the quenching reaction $OD(v''\leq 6) + H_2O \rightarrow OD(v''=0) + H_2O$ is not shown for clarity. The CH_3OOH concentrations are as follows: 1, 0; 2, 4.34×10^{14}; 3, 8.73×10^{14}; 4, 10.94×10^{14} molecules cm^{-3}. (c) OH was produced by photolysis of CH_3OOH. The CH_3OOH concentrations are as follows: 2, 4.88×10^{14}; 3, 6.85×10^{14}; 4, 8.76×10^{14}; 5, 10.66×10^{14}; 6, 15.45×10^{14} molecules cm^{-3}. For the case of $[CH_3OOH] = 0$ (labeled 1), OH was produced by photolyzing a mixture of O_3, $\sim 1 \times 10^{12}$ molecules cm^{-3}, H_2O, ~ 1 Torr, and diluent gas (see Table I) to determine the rate of OH removal in the absence of CH_3OOH.

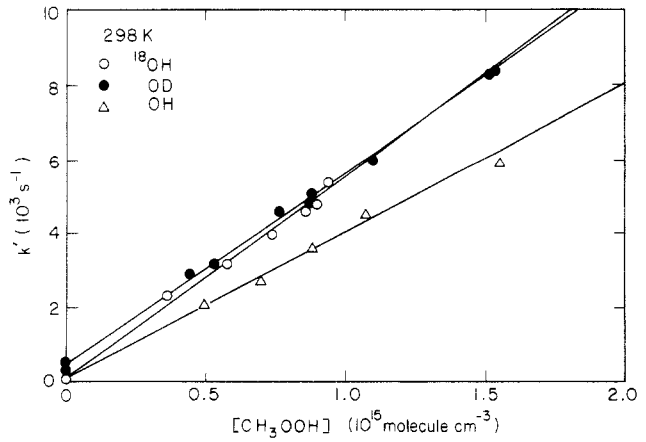

Figure 3. Typical plots of k' versus $[CH_3OOH]$ for ^{18}OH, OD, and OH at 298 K. The value of the slope yields the second-order rate coefficient k. In the case of ^{18}OH or OD this corresponds to k_1, and in the case of OH it corresponds to k_{1a}.

it only reacts with CH_3OOH rather than being quenched. Since the latter possibility seems unlikely, we interpret this result to show negligible (<10%) production of $OH(X^2\Pi, v''\geq 1)$ in CH_3OOH photolysis at 248 nm. It is interesting to note that H_2O_2 photolysis at 248 nm also does not produce vibrationally excited OH.[22]

In a few experiments CH_3OOH was also flash photolyzed in $\sim 6 \times 10^{15}$ molecules cm^{-3} of H_2O. The observed [OH] temporal profiles were strictly exponential, indicating no significant interference from $H + CH_3OOH$ reaction under these conditions of $[H_2O]$. This latter reaction is proposed to give OH as discussed later (H is generated in the initial flash photolysis of H_2O). The measured value of the rate coefficient was the same as that obtained when only CH_3OOH was photolyzed.

Photolysis of O_3 at 248 nm produces approximately 90% $O(^1D)$ and 10% $O(^3P)$.[23,24] Therefore, it is possible that $O(^3P)$ could react with CH_3OOH and generate OH, thereby yielding a lower rate coefficient. As a check for this possibility, a series of experiments were carried out in N_2 where $O(^1D)$ is rapidly quenched to $O(^3P)$.[25,26] The initial ratio of [OH] to $[O(^3P)]$ was ~ 1. The measured value of k_{1a} was the same as in the other experiments, indicating that $O(^3P)$ reaction with CH_3OOH to give OH is slow, as suggested by the studies of Slemr and Warneck.[27]

As mentioned in the Experimental Section, all kinetic measurements were carried out with less than 1×10^{12} molecules cm^{-3} of OH and the $[CH_3OOH]/[OH]$ ratio greater than 1×10^3. Therefore secondary reactions such as $OH + OH \rightarrow H_2O + O$ should not affect the measured value of the rate coefficient. The absence of such reactions was confirmed by varying the initial [OH] by attenuating the photolysis laser beam with neutral density filters (or by varying the xenon flash lamp energy) and observing no change in the measured value of the rate coefficient (see Table II). Also, it is easy to show that on the time scales used for [OH] decay measurements, such radical–radical reactions cannot compete with reaction 1. In experiments where CH_3OOH was photolyzed, CH_3O is also formed. By tuning the probe laser off OH lines, it was confirmed that CH_3O was not being inadvertantly detected (CH_3O has a more diffuse spectrum than OH). Therefore, the presence of CH_3O had no effect on the measured value of the rate coefficient.

The concentration of CH_3OOH was directly measured by UV absorption, either before the reaction mixture entered the reaction cell or after it had exited the reaction cell. The measured value of k_{1a} was independent of the position of the absorption cell used for measuring CH_3OOH concentration. Therefore, the concentration of CH_3OOH in the reaction cell was the same as that determined in the absorption cell. The residence time of the reaction mixture in the cell was varied by altering the linear flow rate of the gas mixture in the range 2–15 cm s^{-1}. No effect on the measured value of k_{1a} was found either at the highest temperature of 348 K studied, indicating that there was no significant thermal decomposition of the peroxide in the reaction cell, or at the lowest temperature, 203 K, showing that sticking of CH_3OOH was not a problem. Kinetic data were not obtained for temperatures much lower than 203 K because of the low vapor pressure (~0.03 Torr) of CH_3OOH and the possible loss of CH_3OOH to the walls of the reaction cell. The measured value of the rate coefficient was also found to be independent of the buffer gas used or the total pressure in the reaction cell. The pressure was varied from 100 to 400 Torr. He, N_2, and SF_6 were used as the buffer gases. In one series of experiments, O_2 was added to the reaction cell to see if it had any effect on the measured value of k_{1a}; none was found. All these variations of experimental parameters and the obtained values of k_{1a} are listed in Table II. Our measured value of k_{1a} is $(3.85 \pm 0.42) \times 10^{-12}$ cm^3 $molecule^{-1}$ s^{-1} at 298

(22) Ondrey, G.; van Veen, N.; Bersohn, R. *J. Chem. Phys.* **1983**, *78*, 3732.
(23) Amimoto, S. T.; Force, A. P.; Wiesenfeld, J. R.; Young, R. H. *J. Chem. Phys.* **1980**, *73*, 1244.
(24) Wine, P. H.; Ravishankara, A. R. *Chem. Phys.* **1982**, *69*, 365.
(25) Wine, P. H.; Ravishankara, A. R. *Chem. Phys. Lett.* **1981**, *77*, 103.
(26) Amimoto, S. T.; Force, A. P.; Gulotty Jr., R. G.; Wiesenfeld, J. R. *J. Chem. Phys.* **1979**, *71*, 3640.
(27) Slemr, F.; Warneck, P. *Int. J. Chem. Kinet.* **1977**, *9*, 267.

TABLE II: Values of the Rate Coefficients for the Reaction of OH, ^{18}OH, and OD with CH_3OOH and the Experimental Conditions Employed in These Determinations

		experimental variables							
		buffer gas			photolysis source		absorption cell		
temp, K	rate coeff[a] ($\pm 1\sigma$), 10^{-12} cm^3 molecule^{-1} s^{-1}	type	press., Torr	linear velocity, cm s^{-1}	type[b]	energy, mJ	position[c]	λ monitor, nm	other conditions[d]
				k_{1a} (OH Reactions)					
348	6.41 + 0.40	He	100	8	XeFL	1500	A	213.9	N_2 purge between XeFL and cell
	3.23 ± 0.34	He	100	8	XeFL	1500	B	213.9	
	av 3.29 ± 0.32								
298	3.73 ± 0.24	He	100	2	XeFL	100	A	228.8	air purge between XeFL and cell
	3.69 ± 0.27	He	100	15	XeFL	100	A	228.8	
	3.70 ± 0.14	He	100	7	XeFL	100	A	228.8	
	3.91 ± 0.08	He	100	7	XeFL	1500	A	213.9	N_2 purge between XeFL and cell, $[H_2O] = 6 \times 10^{15}$
	3.96 ± 0.36	He	100	7	XeFL	1500	A	213.9	N_2 purge between XeFL and cell
	3.69 ± 0.28	He	100	7	XeFL	1500	A	228.8	
	3.77 ± 0.24	He	100	7	XeFL	1500	B	228.8	
	3.97 ± 0.08	N_2	100	2	XeFL	100	A	213.9	
	3.81 ± 0.18 (2)	N_2	300	2	EL	1	A	213.9	
	4.01 ± 0.20	He	300	2	EL	2	A	213.9	$[H_2O] = 1 \times 10^{17}$
	3.77 ± 0.21	He	300	2	EL	1.5	A	228.8	$[H_2O] = 1 \times 10^{17}$
	4.09 ± 0.18	SF_6	400	2	EL	1	A	213.9	
	3.97 ± 0.34 (2)	O_2/He	300	2	EL	2	A	213.9	$[O_2]/[He] = 1$
	3.87 ± 0.15	N_2/He	200	4	EL	2.5	B	213.9	$[OH]/[O^3P] = 1$
	av 3.85 ± 0.23								
244	4.17 ± 0.72	He	100	6	XeFL	1500	A	213.9	N_2 purge between XeFL and cell
	4.48 ± 0.24	He	100	6	XeFL	1500	B	213.9	
	av 4.33 ± 0.54								
223	5.07 ± 0.40	He	100	5	XeFL	1500	A	213.9	
	4.92 ± 0.10	He	100	5	XeFL	1500	B	213.9	
	av 5.00 ± 0.29								
203	5.13 ± 0.19	He	100	5	XeFL	1500	A	213.9	
				$k_1 = k_{1a} + k_{1b}$ (^{18}OH Reactions)					
373	5.06 ± 0.14 (4)	He	200	5	XeFL	1500	A, B	213.9	$[H_2O^{18}] = 3 \times 10^{16}$
298	5.48 ± 0.20 (2)	He	200	4	XeFL	1500	B	213.9	
244	6.45 ± 0.20 (2)	He	200	3	EL	2	B	213.9	$[O_3] = 4 \times 10^{13}$, $[H_2O^{18}] = 1 \times 10^{16}$
223	6.93 ± 0.26 (2)	He	200	3	EL	3	B	213.9	
				$k_1 = k_{1a} + k_{1b}$ (OD Reactions)					
423	4.61 + 0.41 (2)	He	400	5	EL	3	B	213.9	$[D_2] = 2 \times 10^{17}$, $[H_2O] > 2 \times 10^{16}$, $[O_3] < 1 \times 10^{12}$
348	4.97 + 0.48 (4)	He	400	4	EL	4	B	213.9	
298	5.27 + 0.13 (3)	He	400	4	EL	2–5	B	213.9	
249	6.29 + 0.23 (3)	He	400	3	EL	2–4	B	213.9	
298	5.04 + 0.14 (2)	He	400	2	EL	0.2	B	213.9	$[D_2O] = 2 \times 10^{17}$,[e] $[O_3] = 6 \times 10^{14}$
				k_{1a}^D (OD + CH_3OOD)					
298	1.94 + 0.09 (8)	He	100–400	2–7	EL	0.1–3	B	213.9	$[D_2O] = 2 \times 10^{17}$, $[O_3] = 5 \times 10^{14}$
					XeFL	1500	A, B		$[D_2O] = 5 \times 10^{15}$[f]
				k_{1a}^{OH}, $k_{1a}^{OD} + k_{1b}^{OD}$, k_1					
	4.04 + 0.38 (3)[g]								
249	6.41 + 0.40 (3)[h]	He	200	3	EL	0.02	B	213.9	$[D_2] = 4 \times 10^{17}$, $[H_2O] = 2 \times 10^{16}$, $[O_3] = 1 \times 10^{16}$[e]
	6.75 + 0.42 (3)[i]								

[a] Values in parentheses represent the number of determinations of the rate coefficient. Each rate coefficient determination involved the evaluation of 5–10 first-order rate coefficients at different CH_3OOH concentrations. Each first-order rate coefficient involved the measurement of the concentration of the hydroxyl radical at up to 10 different delays times between the photolysis pulse and probe pulse. [b] XeFL = xenon flash lamp, EL = excimer laser, 248 nm. [c] Absorption cell placed after reaction cell (A) and before reaction cell (B). [d] Concentration units in molecules cm^{-3}. [e] Reagent added via movable injector. [f] Deuteriated sample of peroxide. [g] k_{1a}^{OH}. [h] $k_{1a}^{OD} + k_{1b}^{OD}$. [i] k_1.

K and $k_{1a} = (1.78 \pm 0.25) \times 10^{-12} \exp((220 \pm 21)/T)$ cm^3 molecule^{-1} s^{-1}. The errors are 1σ and include estimated uncertainties in the knowledge of CH_3OOH concentration and $\sigma_A = A\sigma_{\ln A}$ in the Arrhenius expression. A plot of ln (k_{1a}) versus $1/T$ is shown in Figure 4.

Measurement of $k_1 = k_{1a} + k_{1b}$. As mentioned earlier, isotopic substitution of either ^{18}O or D in the hydroxyl radical would enable measurement of $k_1 = k_{1a} + k_{1b}$ since the decomposition of CH_2OOH produced in reaction 1b would generate OH rather than ^{18}OH and OD. The results of such measurements are presented below.

$^{18}OH + CH_3OOH$. ^{18}OH was produced either by xenon flash lamp photolysis of $H_2{}^{18}O$ or via the reaction of $O(^1D)$ with $H_2{}^{18}O$ (see Table I). Since the O_3 used to produce $O(^1D)$ is essentially made up of ^{16}O isotope, OH is also formed in the latter case. OH is also expected to be formed due to reaction 1b. Therefore, when a particular rovibrational transition in the (1,0) band is pumped for LIF detection of ^{18}OH, care must be taken to ensure that there is no interference from any nearby OH rovibrational transition. A calculation of the line positions shows that there should be a red shift of $\sim$8.2 cm^{-1} in the rovibrational transitions for the (1,0) band of ^{18}OH relative to that for OH.[21] The fluorescence exci-

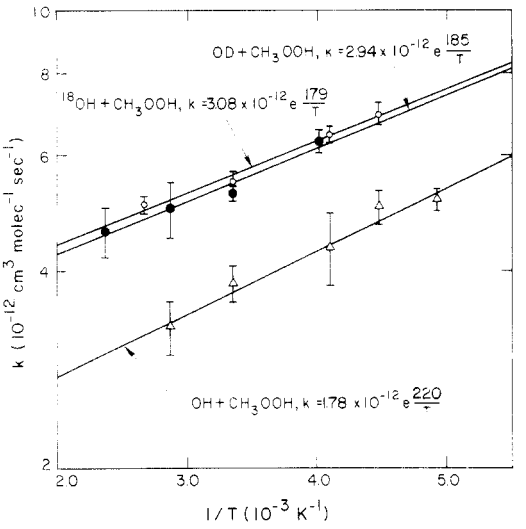

Figure 4. Plots of the second-order rate coefficient k (logarithmic scale) as a function of the reciprocal of the temperature. The data points are averages of many rate coefficient determinations (see Table II). For clarity the computed errors in A and E/R are not shown; they are given in the text.

tation spectrum in the (1,0) band in the region $2814.00 < \lambda_{vac} < 2829.00$ Å was obtained for OH and ^{18}OH. A Torr of H_2O or $H_2{}^{18}O$ was photolyzed in the region 165–185 nm in the presence of 200 Torr of He. A delay of 1 ms was set between the photolysis pulse and the probe laser pulse to allow for complete thermalization of the initially prepared hydroxyl radical by H_2O and He before detection.[28] The resultant fluorescence observed from ($A^2\Sigma^+$, $v'=1$) → ($X^2\Pi, v''=1$) and ($A^2\Sigma^+, v'=0$) → ($X^2\Pi, v''=0$) transitions was normalized to the fluence of the probe and the photolysis beams. The fluorescence excitation spectra obtained are shown in Figure 5, top and middle. It reveals the expected red shift of ~8 cm^{-1} in the ^{18}OH transitions. None of ^{18}OH transitions in this region overlap with OH transitions except the $Q_1(2)$ line, which blends with the $R_2(2)$ line of OH. The kinetics of [^{18}OH] was followed by pumping the $Q_1(1)$ transition, which lies between and is free from $Q_1(1)$ and $Q_1(2)$ transitions of OH, as shown in Figure 5, bottom.

The temporal profile for ^{18}OH concentration in excess CH_3OOH follows a simple first-order loss equation:

$$[^{18}OH]_t = [^{18}OH]_0 e^{-k'_1 t} \qquad (II)$$

where $k'_1 = k_d{}^{18OH} + (k_{1a} + k_{1b})[CH_3OOH]$ and $k_d{}^{18OH}$ is the first-order rate coefficient for the decay of [^{18}OH] in the absence of CH_3OOH. The reaction of $H_2{}^{18}O$ with OH produced via CH_2OOH decomposition or $O(^1D) + H_2{}^{18}O$ reaction is too slow[29] to generate ^{18}OH to any significant extent and to affect the measured value of k_1. Variation of $H_2{}^{18}O$ concentration had no effect on the measured value of k_1, indicating the absence of this interference.

Typical temporal profiles of ^{18}OH concentration are indicated in Figure 2a. The decay of [^{18}OH] was exponential for at least 3 lifetimes, indicating the absence of ^{18}OH regeneration in the above-mentioned reaction. The straight lines shown in the figure represent a weighted linear least-squares fit to the data points and yield k'_1. By plotting the first-order rate coefficient, k'_1, as a function of [CH_3OOH], the values of the second-order rate coefficients for the reaction were obtained. One such plot is shown in Figure 3. The results of our study at 223, 244, 298, and 373 K are summarized in Table II and shown as an Arrhenius plot in Figure 4. Variations of the initial concentration of ^{18}OH, pressure, and O_2 concentration had no effect on the measured value of k_1 rate coefficient. This suggests the absence of secondary reactions. Our measured value of k_1 at 298 K is $(5.48 \pm 0.47) \times 10^{-12}$ cm^3 $molecule^{-1}$ s^{-1} and $k_1 = (3.08 \pm 0.36) \times 10^{-12} \exp((179$

(28) Vaghjiani, G. L.; Ravishankara, A. R. *J. Chem. Phys.* **1987**, *87*, 7050.
(29) Greenblatt, G. D.; Howard, C. J. *J. Phys. Chem.*, in press.

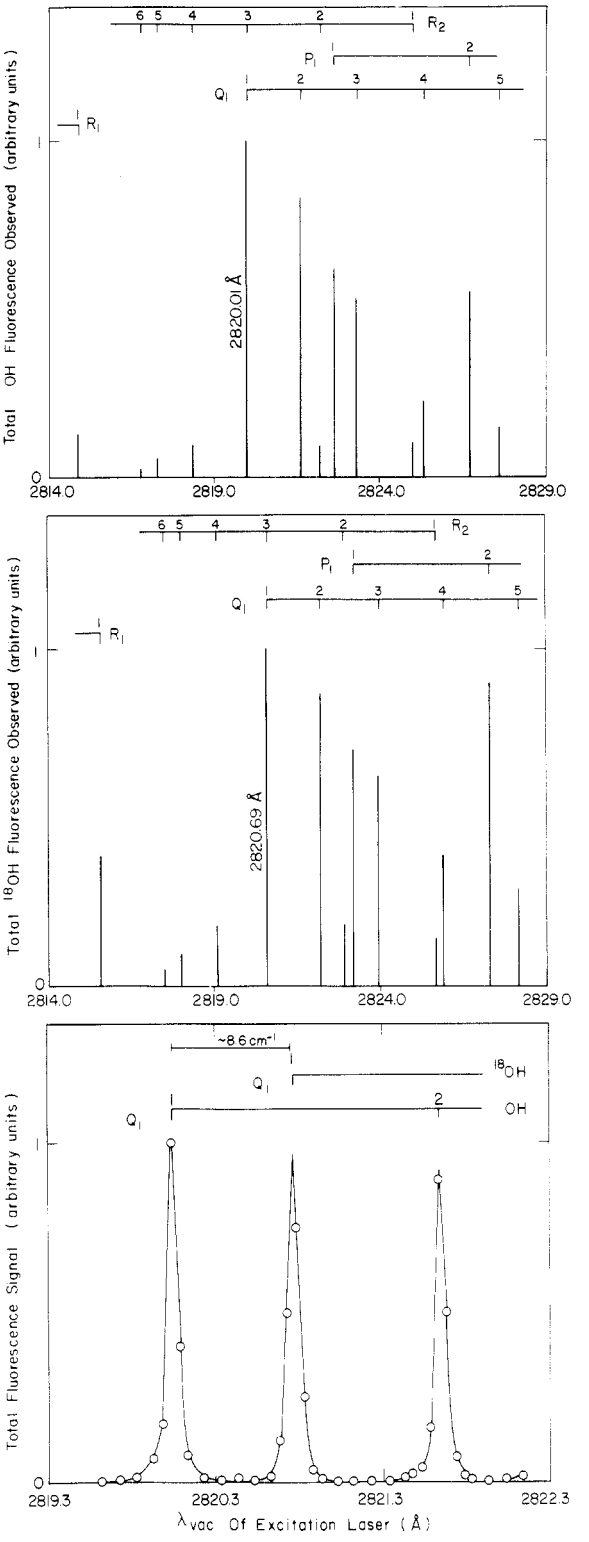

Figure 5. Fluorescence excitation spectrum of OH (top) and ^{18}OH (middle) in the wavelength range 2814.00–2829.00 Å for the (1,0) band. The assignment of each line is shown at the top. The notation shown is that used by Dieke and Crosswhite.[37] H_2O or $H_2{}^{18}O$ (~1 Torr) was photolyzed by Xe flash lamp in 200 Torr of He to generate the hydroxyl radicals. The figures show the expected red shift in the line positions of ^{18}OH relative to OH. The wavelengths of the $Q_1(1)$ transitions of OH and ^{18}OH used to monitor the hydroxyl radical concentration in our experiments are marked. Fluorescence excitation spectrum in the wavelength range 2819.30–2822.30 Å for the (1,0) band obtained in the Xe flash photolysis of ~1 Torr of H_2O and $H_2{}^{18}O$ in 200 Torr of He is shown in the bottom figure. The $Q_1(1)$ transition of ^{18}OH is completely free from the nearby $Q_1(1)$ and $Q_1(2)$ transitions of OH. The measured red shift of the $Q_1(1)$ line is shown. The line width of the transitions of ~1 cm^{-1} corresponds to that of the laser bandwidth. The figure clearly shows that it is possible to monitor ^{18}OH without interference from OH and vice versa.

$\pm 18)/T$) cm^3 $molecule^{-1}$ s^{-1}, where again the error is 1σ and includes estimated errors in the knowledge of CH_3OOH concentration and $\sigma_A = A\sigma_{\ln A}$ in the Arrhenius expression.

$OD + CH_3OOH$. OD was generated by the reaction of $O(^1D)$ with D_2:

$$O(^1D) + D_2 \rightarrow OD(v''\leq 6) + D \quad (6)$$

Ozone, $<1 \times 10^{12}$ molecules cm^{-3}, was photolyzed at 248 nm in the presence of H_2O, $\geq 2 \times 10^{16}$ molecules cm^{-3}. Vibrationally hot OD[30] produced by $O(^1D) + D_2$ was rapidly quenched to the ground vibrational level in the ($X^2\Pi$) state. D atoms produced in reaction 6 can generate OD:

$$D + O_3 \xrightarrow{k_7} OD(v''\leq 13) + O_2 \quad (7)$$

and OD reacts with D_2:

$$OD + D_2 \xrightarrow{k_8} D_2O + D \quad (8)$$

and may exchange with H_2O:

$$OD + H_2O \xrightarrow{k_9} HOD + OH \quad (9)$$

Reactions 7 and 8 constitute a cyclic chain in which OD is regenerated. However, by keeping $[O_3]$ very low, it was possible to suppress reaction 7. In the absence of CH_3OOH, the decay of [OD] was exponential and essentially due to reaction with D_2 (and with H_2O, if any) and thus confirmed the negligible contribution of reaction 7.

The temporal profile of OD concentration in excess CH_3OOH is given by

$$[OD]_t = [OD]_0 e^{-k'_1 t} \quad (III)$$

where $k'_1 = k_d^{OD} + k_8[D_2] + k_9[H_2O] + (k_{1a} + k_{1b})[CH_3OOH]$ and k_d^{OD} is the first-order rate coefficient for the decay of [OD] in the absence of D_2, H_2O, and CH_3OOH, while k_8 and k_9 are the rate coefficients for reactions 8 and 9, respectively. Of course, k_d^{OD} was not directly measured since OD could not be generated in the absence of D_2. Typical first-order decays of [OD] are shown in Figure 2b. The data at very short reaction times, ~ 10 μs, are not shown for clarity. At these short times, the [OD] rose rapidly as $OD(v''\leq 6)$ was quenched by H_2O to form $OD(v''=0)$. In all these experiments OD concentration was monitored by pumping the $Q_1(1)$ or $Q_1(3)$ lines of the (1,0) band in the (A–X) system and measuring the unresolved fluorescence from $(A^2\Sigma^+, v'=1) \rightarrow (X^2\Pi, v''=1)$ and $(A^2\Sigma^+, v'=0) \rightarrow (X^2\Pi, v''=0)$ transitions. There is no interference from OH transitions in detecting OD since there is negligible overlap of the transitions. The noninterference by OH was checked by generating OH via photolysis of H_2O; no signal due to OH was found when the probe laser was tuned onto the OD transition.

The first-order rate coefficient, k'_1, was computed from the slope of a plot of ln [OD] versus time by using a weighted linear least-squares procedure (see Figure 2b). The second-order rate coefficient, k_1, was obtained from the slope of plots of k'_1 versus $[CH_3OOH]$, and a typical example is shown in Figure 3 for $T = 298$ K. The k_1 values determined at 249, 298, 348, and 423 K are given in Table II, and the Arrhenius plot of k_1 is shown in Figure 4. With this source of OD, we were limited to 249 K, since at lower temperatures the vapor pressure of H_2O falls rapidly and we could not introduce sufficient amount of H_2O into the reactor for rapid quenching of the initially prepared $OD(v''\leq 6)$. The value of k_1 at 298 K was measured to be $(5.27 \pm 0.39) \times 10^{-12}$ cm^3 $molecule^{-1}$ s^{-1} and $k_1 = (2.94 \pm 0.38) \times 10^{-12} \exp((185 \pm 24)/T)$ cm^3 $molecule^{-1}$ s^{-1}, and, as before, the indicated errors are 1σ and include estimated systematic errors and $\sigma_A = A\sigma_{\ln A}$ in the Arrhenius expression. The intercept in the plot of k'_1 versus $[CH_3OOH]$ yields a value for $(k_d^{OD} + k_8[D_2] + k_9[H_2O])$. An upper limit for the value of k_9 of $\sim 2 \times 10^{-15}$ at 249 K and of $\sim 2 \times 10^{-14}$ cm^3 $molecule^{-1}$ s^{-1} at 423 K is estimated. This may be compared to a value of $\leq 1 \times 10^{-15}$ cm^3 $molecule^{-1}$ s^{-1} for the rate coefficient for $^{18}OH + H_2O \rightarrow OH + H_2{}^{18}O$ reaction.[29]

Some experiments were carried out by generating OD via the reaction of $O(^1D)$ with D_2O:

$$O(^1D) + D_2O \rightarrow 2OD \quad (10)$$

Due to the rapid isotope exchange between D_2O and CH_3OOH, which generated CH_3OOD, quantitative results could not be obtained. Addition (via a movable injector) of D_2O directly into the reactor just above the photolysis area decreased the isotope exchange. The value of k_1 obtained was $(5.04 \pm 0.39) \times 10^{-12}$ cm^3 $molecule^{-1}$ s^{-1} at 298 K, slightly lower than the value obtained when using $O(^1D) + D_2$ source (the error is 1σ, precision plus systematic). A detailed description of the isotope exchange is given later.

Mechanistic Studies. To obtain information on the pathways involved in the reaction of OH with CH_3OOH, we carried out some experiments that would shed light on the mechanism of reaction 1.

Formation of OH in the Reaction $OD + CH_3OOH \rightarrow CH_2O + HOD + OH$. The intermediate CH_2OOH formed in reaction via channel 1b is expected to be unstable and decompose rapidly into CH_2O and OH. Hence the overall reaction leading to these products may be conveniently written as

$$OD + CH_3OOH \rightarrow CH_2O + HOD + OH$$

Observation of CH_2O or OH formation in the reaction of OD + CH_3OOH would provide additional support to the two-channel mechanism proposed. Though CH_2O can in principle be detected in the present apparatus, its rate of formation and its yield were not observable in the present experiments when CH_2O fluorescence was pumped at 355 nm (third harmonic of the Nd:YAG laser). The difficulty in 355-nm LIF detection of CH_2O lies in its low quantum yield for fluorescence, low absorption cross section at 355 nm, and the minute concentrations of CH_2O available in the present experiments. An alternative approach would be to follow the kinetics of OH production in the above reaction. The possibility of OH formation via a completely different reaction, that of exchange, $CH_3OOH + OD \rightarrow CH_3OOD + OH$, must be considered. Formation of OH via channel 1b and that from the exchange reaction are kinetically indistinguishable. Therefore, we looked for exchange in the related reaction between OD and H_2O_2; the results will be reported in detail in a separate publication dealing with kinetic isotope effects in $OH + H_2O_2$ reaction. No exchange of OD for OH in the reaction $OD + H_2O_2$ was observed. Therefore, we believe that the exchange reaction $OD + CH_3OOH \rightarrow CH_3OOD + OH$ does not take place to any significant extent.

The appearance of OH in $OD + CH_3OOH$ reaction was studied by generating OD via $O(^1D) + D_2$ reaction. In previous experiments where only the decay of [OD] was monitored to obtain k_1, the concentration of O_3 used to photolytically produce $O(^1D)$ was kept very low to minimize $D + O_3$ reaction. We have evidence to suggest that H and D atoms react with CH_3OOH to generate OH (this observation will be discussed later). Therefore, to eliminate OH production from $D + CH_3OOH$ reaction, large concentrations of O_3 were used to completely convert D into OD. Furthermore, to suppress D-atom formation from $OD + D_2$ reaction, these OH appearance experiments were carried out at 249 K where the value of the rate coefficient for reaction 8 is 6 times smaller than that at 298 K. The complete set of reactions that can take place in this OD generation scheme is shown in Table III. Numerical integration of the scheme was carried out to select the optimum concentrations of O_3, D_2, H_2O, and CH_3OOH to quantitatively measure the [OH] appearance rates. It was clear that to obtain a pronounced rise in [OH], the initial concentration of OD had to be at least 10 times greater than that of OH, which is unavoidably produced by CH_3OOH photolysis. Also, ratios of concentrations best suited for these experiments were calculated to be $[O_3]/[CH_3OOH] \sim 10$ and $[D_2]/[H_2O] \sim 20$. The former condition limits the production of OH relative to $O(^1D)$ by a factor of ~ 1600 in the initial photolysis, while the latter condition ensures that $\sim 90\%$ of the initial $O(^1D)$ reacts with D_2. The presence of

(30) Butler, J. E.; Jursich, G. M.; Watson, I. A.; Wiesenfeld, J. R. *J. Chem. Phys.* **1986**, *84*, 5365.

TABLE III: Reactions and the Values of Their Rate Coefficients at 249 K Used in the Numerical Simulations of [OH] Appearance Rates in the Reaction of OD with CH_3OOH

reaction no.	reaction	rate coeff at 249 K,[a] cm^3 molecule^{-1} s^{-1}	ref
6	$O(^1D) + D_2 \rightarrow OD(v''\leq 6) + D$	$k_6 = 1.0 \times 10^{-10}$	13, same as $O(^1D) + H_2$
7	$D + O_3 \rightarrow OD(v''\leq 13) + O_2$	$k_7 = 2.1 \times 10^{-11}$	13, same as $H + O_3$
11	$OD(v'\leq 13) + H_2O \rightarrow\rightarrow OD(v''=0) + H_2O$	$k_{11} = 1.4 \times 10^{-11}$	20
8	$OD + D_2 \rightarrow D_2O + D$	$k_8 = 2.6 \times 10^{-16}$	31, same as $OH + D_2$
$1a^{OD}$	$OD + CH_3OOH \rightarrow CH_3OO + HOD$	$k_{1a}^{OD} = 4.3 \times 10^{-12}$	this work
$1b^{OD}$	$OD + CH_3OOH \rightarrow CH_2OOH + HOD$	$k_{1b}^{OD} = 1.9 \times 10^{-12}$	this work
	$OD \rightarrow$ loss	$k_d^{OD} \sim 50$	this work
9	$OD + H_2O \rightarrow HOD + OH$	$k_9 \leq 2.0 \times 10^{-15}$	this work
12	$OD + O_3 \rightarrow DO_2 + O_2$	$k_{12} = 3.6 \times 10^{-14}$	13, same as $OH + O_3$
13	$DO_2 + O_3 \rightarrow OD + 2O_2$	$k_{13} = 1.4 \times 10^{-15}$	13, same as $HO_2 + O_3$
$1a^{OH}$	$OH + CH_3OOH \rightarrow CH_3OO + HOH$	$k_{1a}^{OH} = 4.3 \times 10^{-12}$	this work
$1b^{OH}$	$OH + CH_3OOH \rightarrow CH_2OOH + HOH$	$k_{1b}^{OH} = 1.9 \times 10^{-12}$	this work
5	$CH_2OOH \xrightarrow{M} CH_2O + OH$	$k_c > 5 \times 10^4$	this work
	$OH \rightarrow$ loss	$k_d^{OH} \sim 50$	this work
14	$OH + D_2 \rightarrow HOD + D$	$k_{14} = 2.6 \times 10^{-16}$	31
15	$OH + O_3 \rightarrow HO_2 + O_2$	$k_{15} = 3.6 \times 10^{-14}$	13
16	$HO_2 + O_3 \rightarrow OH + O_2$	$k_{16} = 1.4 \times 10^{-15}$	13
17	$O(^1D) + H_2O \rightarrow OH(v''\leq 2) + OH$	$k_{17} = 2.2 \times 10^{-10}$	13
18	$OH(v''\leq 2) + H_2O \rightarrow\rightarrow OH(v''=0) + H_2O$	$k_{18} = 1.4 \times 10^{-11}$	20

[a] For first-order process, the units are s^{-1}.

H_2O ensures thermalization of vibrational temperature. Model calculations with O_3 concentrations much higher than 1×10^{16} molecules cm^{-3} indicated nonexponential behavior of the [OD] temporal profile. For much lower concentrations of O_3, the reaction $D + O_3 \rightarrow OD(v''\leq 13) + O_2$ was too slow, and again nonexponential behavior of [OD] profile was expected. Also, expression V for the [OH] temporal profile becomes a poor approximation.

The analytical expression for [OD] is

$$[OD]_t = [OD]_0 e^{-k_{OD}t} \qquad \text{(IV)}$$

where

$$k_{OD} = k_d^{OD} + k_9[H_2O] + k_{12}[O_3] + (k_{1a}^{OD} + k_{1b}^{OD}) \times [CH_3OOH]$$

and that for [OH] is

$$[OH]_t = [OH]_0 e^{-\alpha t} + \frac{(k_{1b}^{OD}[CH_3OOH] + k_9[H_2O])[OD]_0}{\alpha - k_{OD}}(e^{-k_{OD}t} - e^{-\alpha t}) \qquad \text{(V)}$$

where $\alpha = k_d^{OH} + k_{14}[D_2] + k_{15}[O_3] + k_{1a}^{OH}[CH_3OOH]$, and $[OH]_0$ and $[OD]_0$ are the initial concentrations of OH and OD, respectively.

The first term in expression V represents the production of OH in the initial photolysis and its subsequent loss due to reaction with D_2, O_3, CH_3OOH and due to diffusion and reaction with impurities. The second term represents the production of OH due to reaction of OD with CH_3OOH and H_2O, and the concurrent loss of OH due to reactions 1a, 14, and 15 and due to diffusion and reaction impurities with a combined first-order rate coefficient, α, shown above.

In these experiments, ozone was added into the reaction cell via the movable injector, and its concentration was determined at the exit of the reaction cell by using UV absorption at 253.7 nm. The presence of CH_3OOH in the exiting mixture had negligible effect in attenuating the 253.7-nm light. Its concentration is at least 10 times smaller and the absorption cross section $\sim$360 times less than that of ozone. The CH_3OOH concentration in the mixture that did not have ozone was determined by using a 100-cm-long absorption cell and a 213.9-nm zinc line at the entrance of the reaction cell, as described earlier.

For a given $[CH_3OOH]$ in the reaction cell, [OD] and [OH] temporal profiles were measured in back-to-back experiments. In both cases the $Q_1(1)$ line in the (1,0) band was pumped. High J-value transitions of the OH (1,0) band do not interfere with the detection of OD. The same is true for the high J-value transitions of OD (3,0) band when monitoring OH. These are

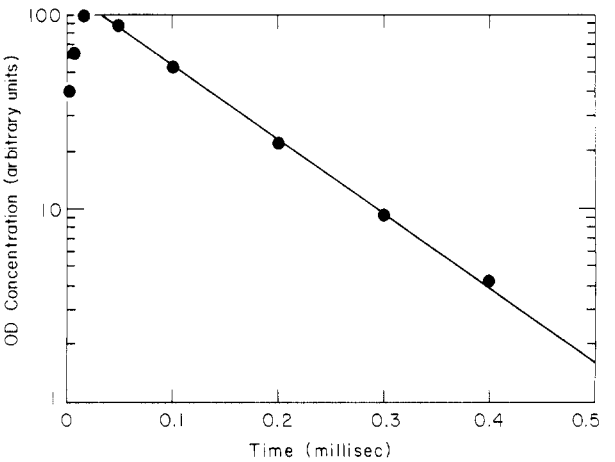

Figure 6. Temporal profile of [OD] obtained via the reaction scheme $O(^1D) + D_2 \rightarrow OD(v''\leq 6) + D$, $D + O_3 \rightarrow OD(v''\leq 13) + O_2$, and $OD(v''\leq 13) + H_2O \rightarrow OD(v''=0) + H_2O$, in the presence of 11.99×10^{14} molecules cm^{-3} of CH_3OOH at 249 K. The initial rise in [OD] is due to the rapid reaction of D with O_3 and quenching of vibrationally hot $OD(v''\leq 13)$ by H_2O. The exponential decay at longer times corresponds to the loss of OD due to reaction. A weighted linear least-squares fit of the data points in this region yields k_{OD}, the first-order rate coefficient for the disappearance of OD.

the potential interferences in detecting OD and OH. Typical temporal profiles of [OD] and [OH] are shown in Figures 6 and 7. The initial rise in [OD] in Figure 6 is due to rapid reaction of D with O_3 and the relaxation of vibrationally hot $OD(v''\leq 13)$ to $OD(v''=0)$ by H_2O. The exponential decay observed at longer times due to reaction of $OD(v''=0)$ typically covered at least 3 lifetimes. The slope of the straight line gives a direct measurement of the first-order rate coefficient, k_{OD}, for the decay of [OD] in the reaction and it is consistent with our measured value of k_1. The temporal profile of Figure 7 was fitted to expression V by using a nonlinear least-squares procedure to obtain the values for both k_{OD} and α. k_{OD} in this latter analysis corresponds to the rate coefficient for [OD] disappearance, and the value obtained was the same as that obtained in the direct mesurement of [OD], consistent with the reaction mechanism proposed above. The second-order rate coefficients obtained from the usual plot of k_{OD} or α versus $[CH_3OOH]$ were in agreement with those values obtained earlier at $T = 249$ K at lower O_3 concentrations and are given in Table II.

A similar experiment aimed at monitoring the temporal profiles of [OH] in the reaction of $^{18}OH + CH_3OOH$ was attempted. The source of ^{18}OH was vacuum photolysis of $H_2{}^{18}O$. The observed

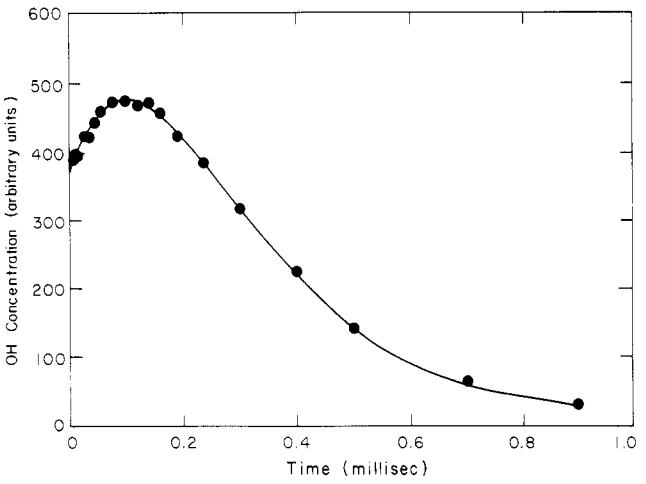

Figure 7. Temporal profile of [OH] in the reaction of OD + CH_3OOH. The [CH_3OOH] and the OD source reaction scheme are the same as those in Figure 6. The solid line is a nonlinear least-squares fit of the data points to expression V (see text). The value obtained for the rate coefficient for OH appearance in this profile is consistent with the value of k_{OD} in Figure 6. The vibrational relaxation of OD($v'' \leq 13$) occurs at very short times, ≤ 20 μs, and is instantaneous on the time scale of the OH formation.

temporal profile was not biexponential of the type given in expression V but was more complex. We believe that the complication arose from the reaction H + $CH_3OOH \rightarrow CH_3OH$ + OH. Very preliminary results of a study on H + CH_3OOH reaction using resonance fluorescence detection of H atoms indicated a rate coefficient of the order of 1.5×10^{-13} cm^3 molecule^{-1} s^{-1} for this reaction, consistent with the observed complex [OH] temporal profile. However, due to unavoidable secondary reactions of H with the photoproducts of CH_3OOH, an accurate rate coefficient measurement was not possible in this experiment. Our high value is an upper limit for the H + CH_3OOH reaction, and it is much higher than that measured by Slemr and Warneck.[27] This investigation was not continued further. It should be noted that when OH production in OD + CH_3OOH reaction was studied, the D atoms formed in the OD source reaction were rapidly removed by reaction with O_3, and hence we observed a much simpler [OH] temporal profile.

Estimation of k_c. To see if CH_2OOH could be stabilized at low temperatures, some experiments were carried out at 205 K. Methyl hydroperoxide was photolyzed at 248 nm in 50 Torr of He, and the [OH] temporal profile monitored starting at short times (i.e., 1 μs). Sufficient stabilization of CH_2OOH would be indicated by a faster decay of [OH] at short reaction times compared to a slower decay at long reaction times. At short times the reaction of OH should be fast compared to its regeneration from stabilized CH_2OOH, i.e., the rate coefficient k_1 would control the [OH] loss if CH_2OOH is not decomposing during this time. At longer times regeneration of OH becomes more important due to the increasing concentration of CH_2OOH and the [OH] loss rate slows down. When CH_2OOH decomposes instantaneously on the time scale of the experiment, channel 1b would be invisible. The reactions that take place in this experiment are

$$OH + CH_3OOH \xrightarrow{k_{1a}} CH_3O_2 + H_2O$$

$$OH + CH_3OOH \xrightarrow{k_{1b}} CH_2OOH + H_2O$$

$$CH_2OOH \xrightarrow{k_c} CH_2O + OH$$

$$OH \xrightarrow{k_d^{OH}} \text{loss}$$

The above reaction scheme was modeled by using numerical Runge Kutta integration, and it showed that if CH_2OOH were to decompose at a rate slower than 5×10^4 s^{-1}, sufficient enhancement ($\geq$25%) in the decay of [OH] should occur initially. Figure 8 shows the computed and measured temporal profiles.

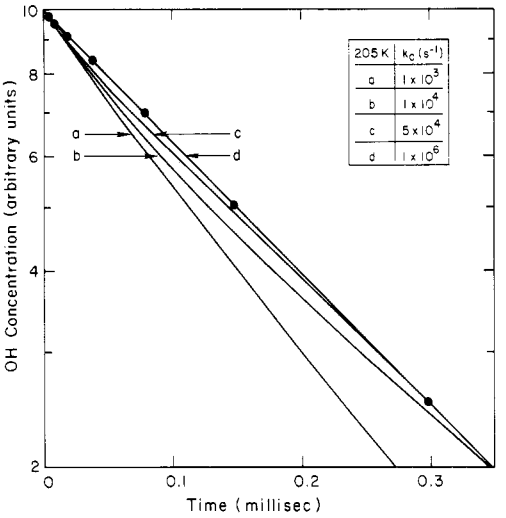

Figure 8. Simulated and measured temporal profiles of [OH] during 248-nm photolysis of CH_3OOH at 205 K in 50 Torr of He. The 1σ error bars on the measured points are smaller than the diameter of the points. The appropriate reaction scheme for the simulation is OH + $CH_3OOH \xrightarrow{k_{1a}} CH_3OO + H_2O$, OH + $CH_3OOH \xrightarrow{k_{1b}} CH_2OOH + H_2O$, $CH_2OOH \xrightarrow{k_c} CH_2OH$ + OH, and OH $\xrightarrow{k_d^{OH}}$ loss. The measured profile is consistent with the rapid decay of CH_2OOH intermediate with $k_c \geq 5 \times 10^4$ s^{-1}. This corresponds to an upper limit for the lifetime of CH_2OOH of $\sim$20 μs at 205 K in 50 Torr of He. k_c greater than 1×10^6 s^{-1} yields a line that is indistinguishable from line d.

A 25% enhancement in the rate would be easily detected in the present apparatus. Therefore, we place a upper limit to the lifetime of CH_2OOH of $\sim$20 μs.

Effect of Isotopic Substitution in OH. Consideration must be given to possible kinetic isotope effects when using isotopically labeled reactants. It is expected that the substitution of OD or ^{18}OH for OH has only a small effect because the bond being broken is that on CH_3OOH. The value of the second-order rate coefficient measured for OD and ^{18}OH reactions with CH_3OOH were, within experimental uncertainties, the same. This observation is consistent with the assumption that the reaction occurs via the abstraction of H from CH_3OOH. Further support for the lack of a kinetic isotope effect in reaction 1 upon substitution in OH was obtained from studying the following related reactions:

$$D_2 + OH \text{ (or } ^{18}OH \text{ or OD)} \rightarrow D + DOH \text{ (or } D^{18}OH \text{ or DOD)} \quad (19)$$

$$HOOH + OH \text{ (or } ^{18}OH \text{ or OD)} \rightarrow HOO + HOH \text{ (or } H^{18}OH \text{ or HOD)} \quad (20)$$

At 298 K the bimolecular rate coefficient for reaction of OD with D_2 was determined to be $(1.88 \pm 0.06) \times 10^{-15}$ cm^3 molecule^{-1} s^{-1} and that for OD (and other isotopes) with HOOH to be $(1.72 \pm 0.10) \times 10^{-12}$ cm^3 molecule^{-1} s^{-1} (the errors are 1σ, precision only). These two values may be compared with those for OH + D_2, $(1.83 \pm 0.12) \times 10^{-15}$ cm^3 molecule^{-1} s^{-1},[31] and OH + H_2O_2, 1.7×10^{-12} cm^3 molecule^{-1} s^{-1}.[13] They clearly show a lack of isotope effect. It may be concluded that the small kinetic isotope effects due to substitution of ^{18}O for ^{16}O and D for H in the hydroxyl radical for its reaction with CH_3OOH (and D_2 or HOOH) are unimportant and too small to be measured in the present study. Therefore, the values of k_1 measured by monitoring OD and ^{18}OH should be the same as that expected for OH reaction with CH_3OOH if OH was not regenerated in channel 1b.

Reaction of CH_3OOD with OD. Mixing D_2O with CH_3OOH produces CH_3OOD. Spectroscopic evidence for exchange was obtained by NMR and IR spectra. ^{1}H NMR ($CDCl_3$) of a sample of methyl hydroperoxide to which some D_2O had been added showed only one feature at δ = 3.87 ppm (sharp, singlet, 3 H). The feature at δ = 8.86 ppm attributed to OH proton was com-

(31) Ravishankara, A. R.; Nicovich, J. M.; Thompson, R. L.; Tully, F. P. *J. Phys. Chem.* **1981**, *85*, 2498.

pletely missing, indicating that the labile proton of the OH group was exchanging with the D_2O. The infrared spectrum of a gas mixture of CH_3OOH in excess D_2O left standing for several minutes did not show a broad feature at $\sim$3600 cm^{-1}, which is attributed to the O–H stretch of CH_3OOH. The corresponding O–D stretch of the exchanged methyl hydroperoxide could not be definitively assigned. However, the shape of the broad C–H stretching feature at $\sim$3000 cm^{-1} was different from that observed in the isotopically pure sample. The O–D stretching band is thought to be hidden under the C–H stretching feature in this region.

Since the product of exchange between CH_3OOH and D_2O should be HOD, we searched for transitions corresponding to isotopically mixed water. Many rovibrational transitions unique to HOD were observed. The intensities of these transitions were much greater than those observed in pure D_2O, which reportedly contained $\sim$0.2% H atoms in the form HOD. Using this sample of CH_3OOD, which may contain some CH_3OOH, we studied the reaction between OD and CH_3OOD by monitoring [OD] temporal profiles. OD was generated by photolysis of CH_3OOD itself. In this case, abstraction of a methyl hydrogen leads to CH_2OOD, which decomposes to CH_2O and OD:

$$OD + CH_3OOD \xrightarrow{k_{1a}^D} CH_3O_2 + D_2O$$

$$OD + CH_3OOD \xrightarrow{k_{1b}^D} CH_2OOD + HOD$$

$$CH_2OOD \xrightarrow[M]{k_c^D} CH_2O + OD$$

Therefore, only k_{1a}^D is measured if the sample is pure CH_3OOD. We obtained a value of $(1.94 \pm 0.19) \times 10^{-12}$ cm^3 $molecule^{-1}$ s^{-1} for k_{1a}^D at 298 K. The error is 1σ, precision plus systematic. This value is an upper limit since any presence of CH_3OOH would make the measured rate coefficient larger. The ratio of k_{1a} to k_{1a}^D is $\sim$2.0 at 298 K, indicating a kinetic isotope effect for the abstraction of H on the peroxy group.

Comparison with Previous Measurement and Discussion of the Rate Coefficient. Assuming that the mechanism given earlier is correct, we obtain $k_{1a} = (3.85 \pm 0.42) \times 10^{-12}$ cm^3 $molecule^{-1}$ s^{-1}, $k_1 = (5.38 \pm 0.44) \times 10^{-12}$ cm^3 $molecule^{-1}$ s^{-1} (average of ^{18}OH and OD studies), and by difference $k_{1b} = (1.53 \pm 0.43) \times 10^{-12}$ cm^3 $molecule^{-1}$ s^{-1} at 298 K. The major errors are in the knowledge of the concentration of CH_3OOH, which is based on our new UV absorption cross sections at 213.9 and 228.8 nm of 2.25×10^{-19} and 1.00×10^{-19} cm^2 $molecule^{-1}$, respectively.[15] Molina and Arguello[16] obtained 3.00×10^{-19} and 1.40×10^{-19} cm^2 $molecule^{-1}$ at these two wavelengths. We have carried out a very careful study of the gas-phase absorption cross sections of CH_3OOH and H_2O_2, where their concentrations were determined via trapping and titration with Fe^{2+} and NaI. The values we obtain for H_2O_2 at various wavelengths agree with the literature values.[13] The cross sections of CH_3OOH measured by using pressure measurements in a slow-flow cell also agree with the values measured via titration. Therefore, we have used only our values rather than take an average of the two studies. Our cross section values have an uncertainty of $\sim$5% (1σ), and the errors shown for the above rate coefficients include this uncertainty. It should be noted that any change in the value of the absorption cross section would have a proportionate change in the values of k_1, k_{1a}, and k_{1b}. The second possible source of error is due to the small amount of diethyl ether that may be present in our sample of CH_3OOH. NMR analysis showed $\sim$3% of diethyl ether, while none was detected in the IR spectra. Prolonged bubbling of a carrier gas should have selectively removed diethyl ether, and we believe that its concentration in the sample used for kinetic measurements was less than 1%. Therefore, we have made no corrections for the possible presence of diethyl ether that reacts with OH; the rate coefficient at 298 K is 1.37×10^{-11} cm^3 $molecule^{-1}$ s^{-1}, with $E/R \sim -200$ K.[32,33]

Niki et al.[14] were the only investigators who have previously measured k_1, k_{1a}, and k_{1b} at 298 K. They performed a chamber experiment where OH was produced via photolysis of CH_3ONO or C_2H_5ONO in air and measured k_1 relative to the reactions

$$OH + C_2H_4 \xrightarrow{k_x} \text{products}$$

$$OH + CH_3CHO \xrightarrow{k_y} \text{products}$$

Assuming $k_x = 8.0 \times 10^{-12}$ cm^3 $molecule^{-1}$ s^{-1} and $k_y = 1.5 \times 10^{-11}$ cm^3 $molecule^{-1}$ s^{-1} at 298 K, they obtain $k_1 = 10.0 \times 10^{-12}$ cm^3 $molecule^{-1}$ s^{-1}. This value is $\sim$90% higher than our value. Since Niki et al. carried out their measurements in air, we added O_2 to our reaction mixture and found no change in the measured value of the rate coefficient. Therefore, the presence of O_2 in Niki et al.'s experiments cannot be the source for this difference. It is difficult to understand a larger rate coefficient in Niki et al.'s experiments unless CH_3OOH also reacted with species other than OH. Niki et al. also carried out extensive product analyses and, based on the mechanism given earlier, deduced the branching ratio to be $k_{1a}/k_{1b} = 1.30 \pm 0.26$. Considering the difficulties in measuring such a ratio in their system, we feel that our ratio of $k_{1a}/k_{1b} = 2.52 \pm 0.36$ is not too bad an agreement with the value of Niki et al. Our branching ratio is derived from the rate coefficient measurements where the pathways have been separated and is more accurate than the individual values of k_{1a} and k_{1b} since the major systematic error, i.e., the measurement of CH_3OOH concentration, does not affect the ratio.

We are the first to measure the temperature dependence of k_1 and k_{1a}. We obtain negative activation energies of $\sim$0.38 and $\sim$0.44 kcal mol^{-1}, respectively for the two rate coefficients. Even channel 1b has zero or a negative activation energy. Channel 1a is similar to the reaction of OH with H_2O_2:

$$OH + H_2O_2 \xrightarrow{k_{20}} HO_2 + H_2O \qquad (20)$$

which exhibits a positive activation energy of $\sim$0.40 kcal mol^{-1}.[13] Also, k_{1a} is more than 4 times larger than the rate coefficient for abstraction of H from H_2O_2 per abstractable H atom (i.e., $0.5k_{20}$). However, the CH_3OO–H bond energy is nearly the same as that in HOO–H [CH_3OO–H bond energy measured by Kondo and Benson[34] is 88.5 kcal mol^{-1}. If the $\Delta H°_f$(298 K) for CH_3O_2 is taken to be 2.7 kcal mol^{-1} as measured by Slagle and Gutman[35] and Khachatryan et al.,[36] we calculate a bond dissociation energy of 85.7 kcal mol^{-1}. HOO–H bond dissociation energy is 87.7 kcal mol^{-1}.] Therefore, it is tempting to consider the possibility of a complex reaction pathway for reaction 1. Three factors suggest otherwise: (a) in the reaction of OD with H_2O_2, we see no evidence for scrambling of H/D, indicating that OH attack on oxygen atom of the peroxide is unlikely; (b) the H-abstraction reaction is so exothermic (ΔH_r(298 K) is $\sim$−33 kcal mol^{-1} for reaction 1a) that if OH attacks an H atom it should go to products without much of a barrier such that even if there is an attractive part to the CH_3OOH–OH interaction, there should be no bound complex; (c) we see a positive deuterium kinetic isotope effect of $\sim$2 at 298 K for hydrogen abstraction from the peroxy group. On the other hand, the negative activation energies observed for the two channels and the overall reaction would be easier to accept in terms of a complex pathway. We do not have conclusive evidence that can point to either of the two possibilities as the actual mechanism of reaction 1.

Atmospheric Implications. Using the measured values of k_1 at atmospheric temperatures along with the rate coefficient for CH_3OOH formation and the photolysis rate of CH_3OOH, the

(32) Wallington, T. J.; Liu, R.; Dagaut, P.; Kurylo, M. J. *Int. J. Chem. Kinet.* **1988**, *20*, 41.

(33) Tully, F. P.; Droege, A. T. *Int. J. Chem. Kinet.* **1987**, *19*, 251.
(34) Kondo, O.; Benson, S. W. *J. Phys. Chem.* **1984**, *88*, 6675.
(35) Slagle, I. R.; Gutman, D. *J. Am. Chem. Soc.* **1985**, *107*, 5342.
(36) Khachatryan, L. A.; Niazyan, O. M.; Mantashyan, A. A.; Vedeneev, V. I.; Teitel'boim, M. A. *Int. J. Chem. Kinet.* **1982**, *14*, 1231.
(37) Dieke, G. H.; Crosswhite, H. M. *J. Quantum Spectrosc. Radiat. Transfer* **1962**, *2*, 97.

concentration of CH_3OOH in various conditions, i.e., polluted and clean troposphere and the stratosphere, can be calculated. Our measured absorption cross sections for CH_3OOH are lower than those of Molina and Arguello[16] by a factor of ~30%, while our value of k_1 is ~90% lower than that of Niki et al.[15] at 298 K. However, we obtain a negative activation energy which yields a value of $k_1 \simeq 6 \times 10^{-12}$ cm^3 molecule^{-1} s^{-1} at the average tropospheric temperature of 260 K. With the changes in the cross sections and k_1, the relative CH_3OOH loss due to photolysis and reaction with OH remains approximately the same. The current major uncertainty in the laboratory data dealing with CH_3OOH is the rate coefficient for the $CH_3O_2 + HO_2$ reaction. On the basis of our measured value for k_1, it might be expected that higher organic peroxides would also have a rate coefficient greater than or equal to k_1.

The two different pathways for reaction 1 have different effects on tropospheric chemistry related to methane oxidation. If reaction 1a takes place, it is equivalent to chain termination by $OH + HO_2$ reaction:

$$CH_3O_2 + HO_2 \rightarrow CH_3OOH + O_2$$

$$OH + CH_3OOH \rightarrow CH_3O_2 + H_2O$$

net $$OH + HO_2 \rightarrow H_2O + O_2$$

On the other hand, reaction 1b leads to formation of CH_2O, which is a net HO_x producer in the atmosphere. In either case, formation of CH_3OOH and its subsequent reaction with OH is a net HO_x sink in the atmosphere. The fate of CH_2OOH formed in reaction 1b under atmospheric conditions of O_2 composition may depend on whether it reacts with O_2 or not. We have estimated that CH_2OOH should decompose to CH_2O and OH within ~20 μs at 205 K, and the decomposition is likely to be faster at higher temperatures. Therefore the reaction of CH_2OOH with O_2:

$$CH_2OOH + O_2 \xrightarrow{k_{21}} \text{products} \qquad (21)$$

must be of the same order of magnitude in the atmosphere to compete with the decomposition, i.e., $k_{21} \geq 1 \times 10^{-14}$ cm^3 molecule^{-1} s^{-1} at atmospheric temperatures. If the reaction is that fast, then depending on the products of reaction 21, CHOOH or CH_2OO can be formed if O_2 abstracts an H atom. We saw no evidence for an increase in k_{1a} in the presence of O_2. This suggests that either reaction 21 is slow, it regenerates OH, or both. Niki et al.[14] saw no evidence to suggest this reaction.

Summary

The reaction of hydroxyl radical with CH_3OOH is fast and proceeds via abstraction of H from the peroxy and methyl groups of the peroxide:

$$CH_3OOH + OH \xrightarrow{k_{1a}} CH_3O_2 + H_2O \qquad (1a)$$

$$CH_3OOH + OH \xrightarrow{k_{1b}} CH_2OOH + H_2O \qquad (1b)$$

$$CH_2OOH \rightarrow CH_2O + OH$$

CH_2OOH formed in reaction 1b decomposes to give OH and CH_2O with a lifetime shorter than 20 μs (at 205 K). Measuring OH loss rates in the reaction $CH_3OOH + OH$, therefore, yielded the rate coefficient for channel 1a only, which was determined to be $k_{1a} = (1.78 \pm 0.25) \times 10^{-12} \exp((220 \pm 21)/T)$ cm^3 molecule^{-1} s^{-1}. For measurement of the overall rate coefficient, $k_1 = k_{1a} + k_{1b}$ for the reaction, isotopically labeled hydroxyl radicals, OD and ^{18}OH were used. The measured rate coefficients using OD and ^{18}OH were, within experimental errors, the same and yielded $k_1 = (2.93 \pm 0.30) \times 10^{-12} \exp((190 \pm 14)/T)$ cm^3 molecule^{-1} s^{-1}. Further evidence for the two-channel mechanism was obtained by direct observation of OH production in the H abstraction reaction, $CH_3OOH + OD \rightarrow CH_2OOH + HOD$ followed by $CH_2OOH \rightarrow CH_2O + OH$. The possibility of OH production via the exchange reaction $CH_3OOH + OD \rightarrow CH_3OOD + OH$ is unlikely since it was not observed in the analogous reaction between H_2O_2 and OD. The reaction of OD with CH_3OOD was half as fast as that between OH and CH_3OOH.

Both reaction 1 and channel 1a show negative activation energies in the temperature range 203-423 K, and the possibility of a complex reaction pathway with an attractive part to the CH_3OOH-OH interaction rather than a simple H atom abstraction mechanism cannot be excluded.

Acknowledgment. We thank J. B. Burkholder and J. J. Orlando for performing the infrared analyses and V. Sankar Iyer for the ^1H NMR analyses. This work was supported by NOAA as part of the National Acid Precipitation Assessment Program.

Registry No. OH, 3352-57-6; CH_3OOH, 3031-73-0; CH_2OOH, 74087-87-9; ^{18}OH, 65553-37-9; H_2O, 7732-18-5; H_2, 1333-74-0; H, 12385-13-6; D_2, 7782-39-0.

Photochemistry of $Mo(CO)_6$ in the Gas Phase

Jane A. Ganske and Robert N. Rosenfeld*

Department of Chemistry, University of California, Davis, California 95616 *(Received: August 10, 1988)*

We report a study of the photochemistry of $Mo(CO)_6$ in the gas phase. Time-resolved infrared laser absorption spectroscopy is used to monitor the vibrational spectroscopy and lifetimes of the coordinatively unsaturated species formed upon photolyses at 351, 248, and 193 nm. The infrared spectra observed indicate that $Mo(CO)_5$ has C_{4v} symmetry, $Mo(CO)_4$ has C_{2v} symmetry, and $Mo(CO)_3$ has C_{3v} symmetry. All three unsaturated species undergo rapid association reactions with $Mo(CO)_6$ and with CO. $Mo(CO)_5$ recombines with CO with a high-pressure limiting rate constant of 2.0 ($\pm$0.2) $\times 10^6$ Torr^{-1} s^{-1}. The corresponding rate constants for $Mo(CO)_4$ and $Mo(CO)_3$ are 7.5 ($\pm$1.5) $\times 10^6$ and 1.8 ($\pm$1.0) $\times 10^7$ Torr^{-1} s^{-1}, respectively.

Introduction

Organometallic reagents have been found to catalyze a variety of chemical transformations. Typically, coordinative unsaturation at the metallic center seems to be required for catalytic activity.[1,2] Information on the structures, lifetimes, and reactivity of coordinatively unsaturated species is thus central in developing a complete understanding of the mechanisms of organo-transition-metal-catalyzed processes.

Unsaturated metal carbonyls, $M(CO)_n$ (where M = Fe, Cr, Mo, etc.), have been reported to catalyze reactions such as the

(1) Collman, J. P.; Hegedus, L. S.; Norton, J. R.; Finke, R. G. *Principles and Applications of Organotransition Metal Chemistry*; University Science Books: Mill Valley, CA, 1987.

(2) Masters, C. *Homogeneous Transition Metal Catalysis*; Chapman and Hall: London, 1981.

0022-3654/89/2093-1959$01.50/0